DESY 11-093 ISSN 0418-9833
June 2011

arXiv:1106.5944v1 [hep-ex] 29 Jun 2011

Measurement of Photon Production in the Very Forward Direction in Deep-Inelastic Scattering at HERA

H1 Collaboration

Abstract

The production of photons at very small angles with respect to the proton beam direction is studied in deep-inelastic positron-proton scattering at HERA. The data are taken with the H1 detector in the years 2006 and 2007 and correspond to an integrated luminosity of $126\ \mathrm{pb}^{-1}$. The analysis covers the range of negative four momentum transfer squared at the positron vertex $6 < Q^2 < 100\ \mathrm{GeV}^2$ and inelasticity $0.05 < y < 0.6$. Cross sections are measured for the most energetic photon with pseudorapidity $\eta > 7.9$ as a function of its transverse momentum p_T^{lead} and longitudinal momentum fraction of the incoming proton x_L^{lead}. In addition, the cross sections are studied as a function of the sum of the longitudinal momentum fraction x_L^{sum} of all photons in the pseudorapidity range $\eta > 7.9$. The cross sections are normalised to the inclusive deep-inelastic scattering cross section and compared to the predictions of models of deep-inelastic scattering and models of the hadronic interactions of high energy cosmic rays.

Submitted to Eur. Phys. J. **C**

F.D. Aaron[5,48], C. Alexa[5], V. Andreev[25], S. Backovic[30], A. Baghdasaryan[38], S. Baghdasaryan[38], E. Barrelet[29], W. Bartel[11], K. Begzsuren[35], A. Belousov[25], P. Belov[11], J.C. Bizot[27], V. Boudry[28], I. Bozovic-Jelisavcic[2], J. Bracinik[3], G. Brandt[11], M. Brinkmann[11], V. Brisson[27], D. Britzger[11], D. Bruncko[16], A. Bunyatyan[13,38], G. Buschhorn[26,†], L. Bystritskaya[24], A.J. Campbell[11], K.B. Cantun Avila[22], F. Ceccopieri[4], K. Cerny[32], V. Cerny[16,47], V. Chekelian[26], J.G. Contreras[22], J.A. Coughlan[6], J. Cvach[31], J.B. Dainton[18], K. Daum[37,43], B. Delcourt[27], J. Delvax[4], E.A. De Wolf[4], C. Diaconu[21], M. Dobre[12,50,51], V. Dodonov[13], A. Dossanov[26], A. Dubak[30,46], G. Eckerlin[11], S. Egli[36], A. Eliseev[25], E. Elsen[11], L. Favart[4], A. Fedotov[24], R. Felst[11], J. Feltesse[10], J. Ferencei[16], D.-J. Fischer[11], M. Fleischer[11], A. Fomenko[25], E. Gabathuler[18], J. Gayler[11], S. Ghazaryan[11], A. Glazov[11], L. Goerlich[7], N. Gogitidze[25], M. Gouzevitch[11,45], C. Grab[40], A. Grebenyuk[11], T. Greenshaw[18], B.R. Grell[11], G. Grindhammer[26], S. Habib[11], D. Haidt[11], C. Helebrant[11], R.C.W. Henderson[17], E. Hennekemper[15], H. Henschel[39], M. Herbst[15], G. Herrera[23], M. Hildebrandt[36], K.H. Hiller[39], D. Hoffmann[21], R. Horisberger[36], T. Hreus[4,44], F. Huber[14], M. Jacquet[27], X. Janssen[4], L. Jönsson[20], H. Jung[11,4,52], M. Kapichine[9], I.R. Kenyon[3], C. Kiesling[26], M. Klein[18], C. Kleinwort[11], T. Kluge[18], R. Kogler[11], P. Kostka[39], M. Kraemer[11], J. Kretzschmar[18], K. Krüger[15], M.P.J. Landon[19], W. Lange[39], G. Laštovička-Medin[30], P. Laycock[18], A. Lebedev[25], V. Lendermann[15], S. Levonian[11], K. Lipka[11,50], B. List[11], J. List[11], R. Lopez-Fernandez[23], V. Lubimov[24], L. Lytkin[9], A. Makankine[9], E. Malinovski[25], P. Marage[4], H.-U. Martyn[1], S.J. Maxfield[18], A. Mehta[18], A.B. Meyer[11], H. Meyer[37], J. Meyer[11], S. Mikocki[7], I. Milcewicz-Mika[7], F. Moreau[28], A. Morozov[9], J.V. Morris[6], M. Mudrinic[2], K. Müller[41], Th. Naumann[39], P.R. Newman[3], C. Niebuhr[11], D. Nikitin[9], G. Nowak[7], K. Nowak[11], J.E. Olsson[11], D. Ozerov[24], P. Pahl[11], V. Palichik[9], I. Panagoulias[l,11,42], M. Pandurovic[2], Th. Papadopoulou[l,11,42], C. Pascaud[27], G.D. Patel[18], E. Perez[10,45], A. Petrukhin[11], I. Picuric[30], S. Piec[11], H. Pirumov[14], D. Pitzl[11], R. Plačakytė[12], B. Pokorny[32], R. Polifka[32], B. Povh[13], V. Radescu[14], N. Raicevic[30], T. Ravdandorj[35], P. Reimer[31], E. Rizvi[19], P. Robmann[41], R. Roosen[4], A. Rostovtsev[24], M. Rotaru[5], J.E. Ruiz Tabasco[22], S. Rusakov[25], D. Šálek[32], D.P.C. Sankey[6], M. Sauter[14], E. Sauvan[21], S. Schmitt[11], L. Schoeffel[10], A. Schöning[14], H.-C. Schultz-Coulon[15], F. Sefkow[11], L.N. Shtarkov[25], S. Shushkevich[26], T. Sloan[17], I. Smiljanic[2], Y. Soloviev[25], P. Sopicki[7], D. South[11], V. Spaskov[9], A. Specka[28], Z. Staykova[4], M. Steder[11], B. Stella[33], G. Stoicea[5], U. Straumann[41], T. Sykora[4,32], P.D. Thompson[3], T.H. Tran[27], D. Traynor[19], P. Truöl[41], I. Tsakov[34], B. Tseepeldorj[35,49], J. Turnau[7], K. Urban[15], A. Valkárová[32], C. Vallée[21], P. Van Mechelen[4], Y. Vazdik[25], D. Wegener[8], E. Wünsch[11], J. Žáček[32], J. Zálešák[31], Z. Zhang[27], A. Zhokin[24], H. Zohrabyan[38], and F. Zomer[27]

[1] *I. Physikalisches Institut der RWTH, Aachen, Germany*
[2] *Vinca Institute of Nuclear Sciences, University of Belgrade, 1100 Belgrade, Serbia*
[3] *School of Physics and Astronomy, University of Birmingham, Birmingham, UK[b]*
[4] *Inter-University Institute for High Energies ULB-VUB, Brussels and Universiteit Antwerpen, Antwerpen, Belgium[c]*
[5] *National Institute for Physics and Nuclear Engineering (NIPNE) , Bucharest, Romania[m]*
[6] *Rutherford Appleton Laboratory, Chilton, Didcot, UK[b]*
[7] *Institute for Nuclear Physics, Cracow, Poland[d]*
[8] *Institut für Physik, TU Dortmund, Dortmund, Germany[a]*
[9] *Joint Institute for Nuclear Research, Dubna, Russia*
[10] *CEA, DSM/Irfu, CE-Saclay, Gif-sur-Yvette, France*
[11] *DESY, Hamburg, Germany*

[12] *Institut für Experimentalphysik, Universität Hamburg, Hamburg, Germany*[a]
[13] *Max-Planck-Institut für Kernphysik, Heidelberg, Germany*
[14] *Physikalisches Institut, Universität Heidelberg, Heidelberg, Germany*[a]
[15] *Kirchhoff-Institut für Physik, Universität Heidelberg, Heidelberg, Germany*[a]
[16] *Institute of Experimental Physics, Slovak Academy of Sciences, Košice, Slovak Republic*[f]
[17] *Department of Physics, University of Lancaster, Lancaster, UK*[b]
[18] *Department of Physics, University of Liverpool, Liverpool, UK*[b]
[19] *Queen Mary and Westfield College, London, UK*[b]
[20] *Physics Department, University of Lund, Lund, Sweden*[g]
[21] *CPPM, Aix-Marseille Université, CNRS/IN2P3, Marseille, France*
[22] *Departamento de Fisica Aplicada, CINVESTAV, Mérida, Yucatán, México*[j]
[23] *Departamento de Fisica, CINVESTAV IPN, México City, México*[j]
[24] *Institute for Theoretical and Experimental Physics, Moscow, Russia*[k]
[25] *Lebedev Physical Institute, Moscow, Russia*[e]
[26] *Max-Planck-Institut für Physik, München, Germany*
[27] *LAL, Université Paris-Sud, CNRS/IN2P3, Orsay, France*
[28] *LLR, Ecole Polytechnique, CNRS/IN2P3, Palaiseau, France*
[29] *LPNHE, Université Pierre et Marie Curie Paris 6, Université Denis Diderot Paris 7, CNRS/IN2P3, Paris, France*
[30] *Faculty of Science, University of Montenegro, Podgorica, Montenegro*[n]
[31] *Institute of Physics, Academy of Sciences of the Czech Republic, Praha, Czech Republic*[h]
[32] *Faculty of Mathematics and Physics, Charles University, Praha, Czech Republic*[h]
[33] *Dipartimento di Fisica Università di Roma Tre and INFN Roma 3, Roma, Italy*
[34] *Institute for Nuclear Research and Nuclear Energy, Sofia, Bulgaria*[e]
[35] *Institute of Physics and Technology of the Mongolian Academy of Sciences, Ulaanbaatar, Mongolia*
[36] *Paul Scherrer Institut, Villigen, Switzerland*
[37] *Fachbereich C, Universität Wuppertal, Wuppertal, Germany*
[38] *Yerevan Physics Institute, Yerevan, Armenia*
[39] *DESY, Zeuthen, Germany*
[40] *Institut für Teilchenphysik, ETH, Zürich, Switzerland*[i]
[41] *Physik-Institut der Universität Zürich, Zürich, Switzerland*[i]

[42] *Also at Physics Department, National Technical University, Zografou Campus, GR-15773 Athens, Greece*
[43] *Also at Rechenzentrum, Universität Wuppertal, Wuppertal, Germany*
[44] *Also at University of P.J. Šafárik, Košice, Slovak Republic*
[45] *Also at CERN, Geneva, Switzerland*
[46] *Also at Max-Planck-Institut für Physik, München, Germany*
[47] *Also at Comenius University, Bratislava, Slovak Republic*
[48] *Also at Faculty of Physics, University of Bucharest, Bucharest, Romania*
[49] *Also at Ulaanbaatar University, Ulaanbaatar, Mongolia*
[50] *Supported by the Initiative and Networking Fund of the Helmholtz Association (HGF) under the contract VH-NG-401.*
[51] *Absent on leave from NIPNE-HH, Bucharest, Romania*

[52] *On leave of absence at CERN, Geneva, Switzerland*

[†] *Deceased*

[a] *Supported by the Bundesministerium für Bildung und Forschung, FRG, under contract numbers 05H09GUF, 05H09VHC, 05H09VHF, 05H16PEA*
[b] *Supported by the UK Science and Technology Facilities Council, and formerly by the UK Particle Physics and Astronomy Research Council*
[c] *Supported by FNRS-FWO-Vlaanderen, IISN-IIKW and IWT and by Interuniversity Attraction Poles Programme, Belgian Science Policy*
[d] *Partially Supported by Polish Ministry of Science and Higher Education, grant DPN/N168/DESY/2009*
[e] *Supported by the Deutsche Forschungsgemeinschaft*
[f] *Supported by VEGA SR grant no. 2/7062/ 27*
[g] *Supported by the Swedish Natural Science Research Council*
[h] *Supported by the Ministry of Education of the Czech Republic under the projects LC527, INGO-LA09042 and MSM0021620859*
[i] *Supported by the Swiss National Science Foundation*
[j] *Supported by CONACYT, México, grant 48778-F*
[k] *Russian Foundation for Basic Research (RFBR), grant no 1329.2008.2*
[l] *This project is co-funded by the European Social Fund (75%) and National Resources (25%) - (EPEAEK II) - PYTHAGORAS II*
[m] *Supported by the Romanian National Authority for Scientific Research under the contract PN 09370101*
[n] *Partially Supported by Ministry of Science of Montenegro, no. 05-1/3-3352*

1 Introduction

Measurements of particle production at very small angles with respect to the proton beam direction (forward direction) in positron-proton collisions are important for the understanding of proton fragmentation. These measurements also provide important constraints for the modelling of the high energy air showers and thereby are very valuable for the understanding of high energy cosmic ray data. The H1 and ZEUS experiments at the $e^{\pm}p$ collider HERA have published several analyses on the production of forward protons and neutrons which carry a large fraction of the longitudinal momentum of the incoming proton [1–5]. These measurements probe different mechanisms related to the baryon production in forward direction, such as elastic scattering of the proton, diffractive dissociation, pion exchange and string fragmentation. In particular, these measurements test the hypothesis of limiting fragmentation [6, 7], according to which, in the high-energy limit, the cross section for the inclusive production of particles in the target fragmentation region is independent of the incident projectile energy. This hypothesis implies, that in deep-inelastic scattering (DIS) forward particle production cross sections are independent of the Bjorken-x and the virtuality of the exchanged photon Q^2.

The measurement of the photon production in the forward direction can provide new input to the understanding of proton fragmentation, and is complementary to forward baryon measurements. The production of photons and π^0 mesons in the proton fragmentation region has been studied in $\bar{p}p$ and pp collisions at SPS and the LHC colliders [8, 9]. The analysis presented here is the first measurement of very forward photons in DIS $e^{+}p$ collisions at HERA. The photons are detected at very small angles below 0.75 mrad with respect to proton beam direction. It relies on the upgraded H1 Forward Neutron Calorimeter (FNC) which includes an electromagnetic section.

2 Experimental Procedure and Data Analysis

The data used in this analysis were collected with the H1 detector at HERA in the years 2006 and 2007 and correspond to an integrated luminosity of $126\ \mathrm{pb}^{-1}$. During the period corresponding to the analysis data set HERA collided positrons and protons with energies of $E_e = 27.6$ GeV and $E_p = 920$ GeV, respectively, corresponding to a centre-of-mass energy of $\sqrt{s} = 319$ GeV.

2.1 H1 detector

A detailed description of the H1 detector can be found elsewhere [10–15]. Only the detector components relevant to this analysis are briefly described here. The origin of the right-handed H1 coordinate system is the nominal $e^{+}p$ interaction point. The direction of the proton beam defines the positive z axis; the polar angle θ is measured with respect to this axis. Transverse momenta are measured in the x–y plane. The pseudorapidity is defined by $\eta = -\ln(\tan\frac{\theta}{2})$ and is measured in the lab frame. The polar angles $\theta < 0.75$ mrad correspond to pseudorapidity range $\eta > 7.9$.

The interaction region is surrounded by a two-layer silicon strip detector and two large concentric drift chambers. Charged particle momenta are measured in the angular range $25^\circ < \theta < 155^\circ$. The tracking system is surrounded by a finely segmented Liquid Argon (LAr) calorimeter, which covers the polar angle range of $4^\circ < \theta < 154^\circ$ with full azimuthal acceptance. The LAr calorimeter consists of an electromagnetic section with lead absorber and a hadronic section with steel absorber. The total depth of the LAr calorimeter ranges from 4.5 to 8 hadronic interaction lengths. The backward region ($153^\circ < \theta < 177.8^\circ$) is covered by a lead/scintillating-fibre calorimeter (SpaCal). Its main purpose is the detection of the scattered positron. The energy resolution for positrons is $\sigma(E)/E \approx 7.1\%/\sqrt{E[\mathrm{GeV}]} \oplus 1\%$, as determined in test beam measurements [14]. The LAr and SpaCal calorimeters are surrounded by a superconducting solenoid which provides a uniform magnetic field of 1.16 T along the beam direction.

The luminosity is measured via the Bethe-Heitler Bremsstrahlung process $ep \to e'p\gamma$, the final state photon being detected in a tungsten/quartz-fibre sampling calorimeter at $z = -103$ m.

The data sample of this analysis was collected using triggers which require the scattered positron to be measured in the SpaCal. The trigger efficiency is about 96% for the analysis phase space as determined from data using independently triggered data.

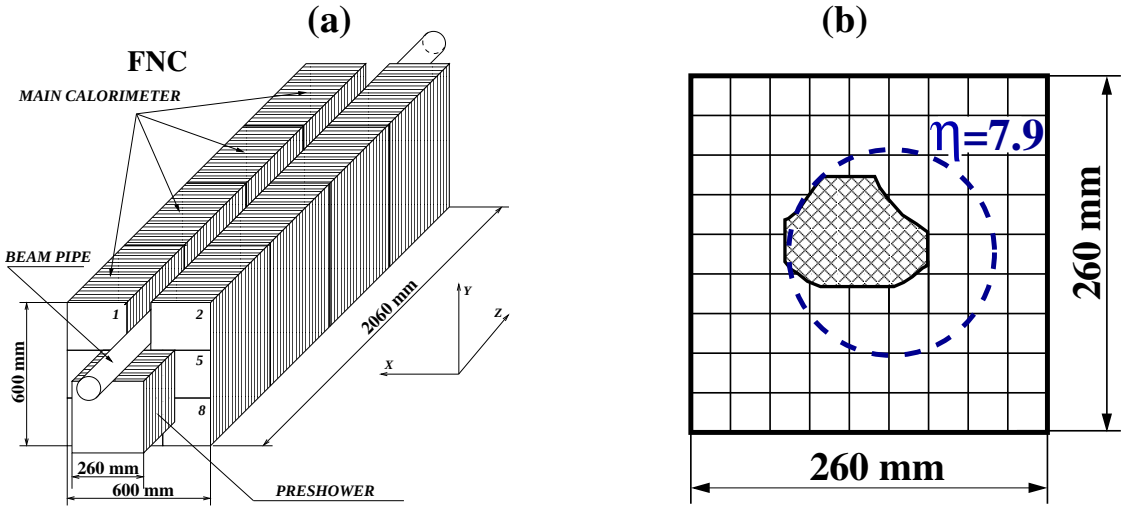

Figure 1: (a) A schematic view of the H1 FNC. (b) Layout of 9 vertical and 9 horizontal readout strips of the Preshower Calorimeter. The hatched area shows the geometrical acceptance window defined by the beam-line elements. The area corresponding to $\eta > 7.9$ is indicated by dashed circle.

2.2 Detection of forward neutral particles

Neutral particles produced at very small polar angles can be detected in the FNC calorimeter, which is situated at a polar angle of 0°, at $z = +106$ m from the interaction point. A schematic view of the H1 FNC used during the HERA-II running period is shown in figure 1a. A detailed description of the detector is given in [5]. The FNC consists of the Main Calorimeter and the

Preshower Calorimeter. The Main Calorimeter is a lead-scintillator sandwich calorimeter with a total length of 8.9 nuclear interaction lengths. The Preshower Calorimeter is a 40 cm long lead-scintillator sandwich calorimeter. The length corresponds to about 60 radiation lengths. The Preshower Calorimeter is composed of 24 planes: the first 12 planes each consist of a lead plate of 7.5 mm thickness and a scintillator plate of 2.6 mm thickness. The second 12 planes each consist of a lead plate of 14 mm thickness and a scintillator plate of 5.2 mm thickness. The transverse size of the scintillating plates is $26 \times 26\ \mathrm{cm}^2$. Each scintillating plate has 45 grooves with 1.2 mm wavelength shifter fibres attached down one side. The orientation of fibres alternates from horizontal to vertical in consecutive planes. For each plane, the fibres are bundled into nine strips of five fibres each. Longitudinally, all strips are combined leading to 9 vertical and 9 horizontal towers which are finally connected to 18 photomultipliers.

The acceptance of the FNC is defined by the aperture of the HERA beam-line magnets and is limited to scattering angles of $\theta \lesssim 0.8$ mrad with approximately 30% azimuthal coverage. The geometrical acceptance window of the FNC is shown in figure 1b together with the layout of the Preshower Calorimeter readout strips.

The longitudinal segmentation of the FNC allows efficient discrimination of photons from hadrons. The photon reconstruction algorithm is based on the fact that electromagnetic showers are fully contained in the Preshower Calorimeter with no energy deposits above the noise level in the Main Calorimeter. For high energy neutrons most of the energy is contained in the Main Calorimeter. However, low energy neutrons deposit large fractions of their energy in the Preshower Calorimeter. The fraction of neutrons which can be misidentified as photons is about 10% for 90 GeV neutrons decreasing to below 1% for neutrons with an energy of 200 GeV, as determined from the Monte Carlo (MC) simulation. The energy deposits in the FNC which are contained in the Preshower Calorimeter are classified as electromagnetic clusters and are considered as photon candidates. The detection and reconstruction efficiency for photons in the measured angular range $\theta < 0.75$ mrad, as estimated from MC simulation, is about 85% for 100 GeV photons increasing to 95% for photons with energies of 900 GeV. Losses are mainly due to interactions with the beampipe.

All modules of the FNC were initially calibrated at CERN using 120-230 GeV electron and 120-350 GeV hadron beams. After the calorimeter was installed at DESY, the stability of calibration constants was monitored using interactions between the proton beam and residual gas in the beam pipe, as described in [5]. Refined calibration constants for electromagnetic showers are determined using an iterative procedure based on the assumption that the maximum photon energy, E_γ^{max}, as measured in the Preshower Calorimeter, is expected to be equal to the proton beam energy in case of unlimited statistics. This calibration procedure also utilises data from HERA runs with reduced proton beam energies of 460 GeV and 575 GeV. The validity of this algorithm is tested with MC simulation.

The measured photon energy spectra for the three proton beam energies are displayed in figure 2a. The correlation between the beam energy and the maximum photon energy E_γ^{max} as determined by the iterative procedure and after applying the calibration is shown in figure 2b. Using this calibration procedure, the linearity of the energy response and the absolute energy scale are verified to a precision of 5%.

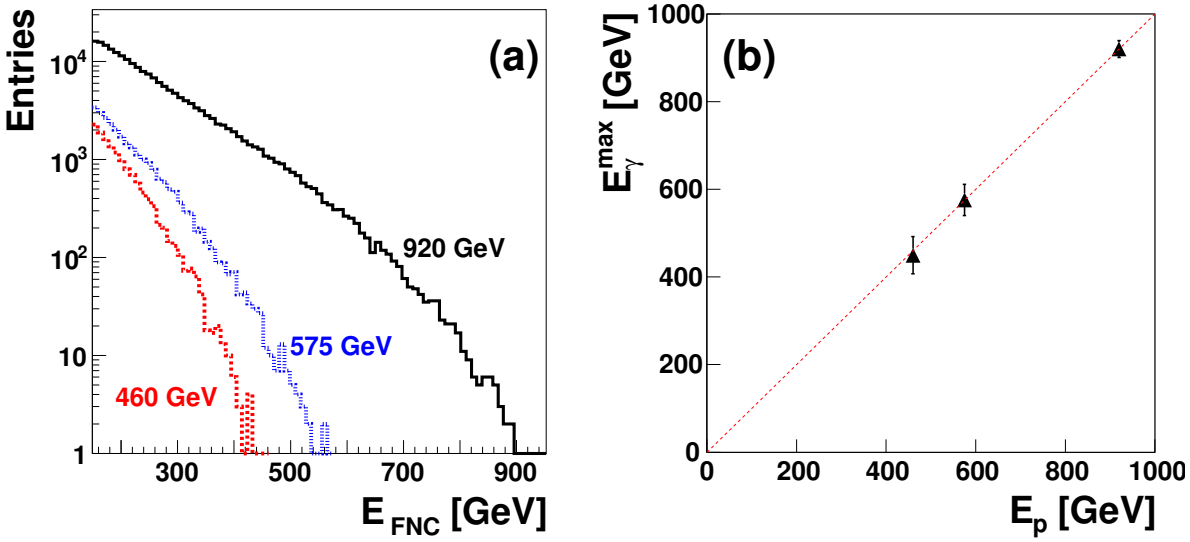

Figure 2: (a) The measured photon energy spectra for three proton beam energies. (b) The correlation between the proton beam energy and E_γ^{max}.

The energy resolution of the FNC calorimeter for electromagnetic showers is $\sigma(E)/E \approx 20\%/\sqrt{E\,[\mathrm{GeV}]} \oplus 2\%$, as determined in test beam measurements. The spatial resolution for single electromagnetic showers and for those hadronic showers which started to develop in the Preshower Calorimeter is about 2 mm.

2.3 Kinematics and event selection

The kinematic variables used to describe high energy DIS interactions are the exchanged photon virtuality Q^2, the inelasticity y and the Bjorken scaling variable x_{Bj}. They are defined as

$$Q^2 = -q^2\,, \qquad x_{Bj} = \frac{Q^2}{2p\cdot q}\,, \qquad y = \frac{p\cdot q}{p\cdot k}\,, \tag{1}$$

where p, k and q are the four-momenta of the incident proton, the incident positron and the virtual photon, respectively.

The selection of DIS events is based on the identification of the scattered positron as the most energetic compact calorimetric deposit in the SpaCal with an energy $E'_e > 11$ GeV and a polar angle $156^\circ < \theta'_e < 175^\circ$. The z coordinate of the primary event vertex is required to be within ± 35 cm of the nominal position of the interaction point. The hadronic final state is reconstructed using an energy flow algorithm which combines charged particles measured in the tracker with information from the SpaCal and LAr calorimeters [17,18]. To suppress events with hard initial state radiation, as well as events originating from non-e^+p interactions, the quantity $\sum E - p_z$, summed over all reconstructed final state particles including the positron, is required to lie between 35 GeV and 70 GeV. This quantity, which uses the energy and longitudinal momentum component of each final state particle, is expected to be twice the electron beam energy for fully

contained events. In addition, events are restricted to the kinematic range $6 < Q^2 < 100$ GeV^2 and $0.05 < y < 0.6$. These variables are reconstructed using a technique which optimises the resolution throughout the measured y range, exploiting information from both the scattered positron and the hadronic final state [16]. The data sample of the DIS events contains about 9.2 million events.

Events containing forward photons are selected by requiring an electromagnetic cluster in the FNC with a pseudorapidity above 7.9 and an energy above 92 GeV, which corresponds to the longitudinal momentum fraction $x_L = E_\gamma/E_p > 0.1$, where E_p and E_γ are the proton beam and forward photon energy, respectively. The data sample contains 78740 events.

In this analysis normalised differential cross sections are measured for the most energetic forward photon (leading photon) with pseudorapidity $\eta > 7.9$ as a function of its longitudinal momentum fraction x_L^{lead} and transverse momentum p_T^{lead}, in the range $0.1 < x_L^{lead} < 0.7$. Cross sections are also measured as a function of the sum of longitudinal momentum fractions of all forward photons with $\eta > 7.9$, $x_L^{sum} = \sum x_L$, in the range $0.1 < x_L^{sum} < 0.95$. These cross sections are given as the fraction of DIS events having forward photon in the η–x_L regions given above. Finally, the ratio of the forward photon production cross section to the inclusive DIS cross section is presented as a function of Q^2 and x_{Bj}.

2.4 Monte Carlo simulations and corrections to the data

Monte Carlo simulations are used to correct the data for the effects of detector acceptance, inefficiencies, migrations between measurement bins due to finite detector resolution and QED radiation from the positron. All generated events are passed through a GEANT3 [19] based simulation of the H1 apparatus and are then processed using the same reconstruction and analysis chain as is used for the data.

The DJANGOH [20] program is used to generates inclusive DIS events. It is based on leading order electroweak cross sections and takes into account QCD effects up to order α_s. Higher order QCD effects are simulated using leading log parton showers as implemented in LEPTO [21], or using the Colour Dipole Model (CDM) as implemented in ARIADNE [22]. Subsequent hadronisation effects are modelled using the Lund string fragmentation model as implemented in JETSET [23, 24]. Higher order electroweak processes are simulated using an interface to HERACLES [25]. The LEPTO program includes the simulation of soft colour interactions (SCI) [26], in which the production of diffraction-like configurations is enhanced via non-perturbative colour rearrangements between the outgoing partons. In the measured x_L range, omitting the SCI in the LEPTO would decrease the predicted yield of forward photons by 5% at lowest x_L and 2% at highest x_L. The simulation with CDM uses the parameters tuned to describe H1 forward jet measurements [27]. The DJANGOH MC simulations are calculated using the H1PDF 2009 parameterisation [28] of the parton distributions in the proton. In the following, the predictions based on LEPTO and ARIADNE are denoted LEPTO and CDM, respectively.

The measurements are also compared with the predictions of several hadronic interaction models which are commonly used for the simulation of cosmic ray air shower cascades:

EPOS [29], QGSJET 01 [30,31], QGSJET II [32,33] and SIBYLL [34,35]. These phenomenological models, based on general principles such as unitarity and analyticity of scattering amplitudes, are combined with perturbative QCD predictions for high-p_T processes to obtain a description of the final state. The programs are interfaced with the PHOJET program [36] for the simulation of e^+p interactions.

In all of these models, the main source of forward photons is the decay of π^0 mesons produced from the hadronisation of the proton remnant. The measured distributions may contain background arising from several sources. The background from photoproduction processes, where the positron is scattered into the backward beam-pipe and a particle from the hadronic final state fakes the positron signature in the SpaCal, is estimated using the PHOJET MC generator and found to be negligible. The selected sample may contain background from neutrons reconstructed as electromagnetic clusters as explained above. For cluster energies above 92 GeV this background is found to be negligible according to the MC simulation. The background from the random coincidences of DIS events with a beam-related background signals in the FNC is estimated by combining DIS events with forward particles in adjacent bunch-crossings. It is found to be smaller than 1%. The background contributions are not subtracted from themeasured cross sections.

Two or more particles entering the FNC are reconstructed as a single cluster due to the relatively large size of the FNC readout modules in combination with a small geometrical acceptance window. According to the MC simulation, low energetic clusters reconstructed in the FNC mainly originate from single photons. The contribution from two photons increases almost linearly from 10% at about 450 GeV to 80% at 900 GeV (the contribution from three and more photons is below 1%). Therefore, the measurement of the cross section of single photon production is limited to $x_L < 0.7$, while the measurement of the total forward photon production cross section is extended to larger x_L.

Factors determined from MC are used to correct distributions at the level of reconstructed particles back to the hadron level on a bin-by-bin basis. These correction factors include the effects of QED radiation from the positron. For the calculation of the correction factors the simulations are reweighted to describe the x_L distributions of the data. The average of the correction factors determined from LEPTO and CDM is used. The size of the correction factors varies between 2 and 3.5 for x_L^{lead}, between 3 and 4 for x_L^{sum}, between 2.5 and 12 for p_T^{lead} and are about 3.2 for the Q^2 and x_{Bj} distributions. They are dominated by the non-uniform azimuthal acceptance of the FNC, which is about 30% on average. The bin purities, defined as the fraction of events reconstructed in a particular bin that originate from that bin on hadron level, vary between 75% and 95%.

2.5 Systematic uncertainties

The systematic uncertainties on the cross section measurements are determined using MC simulations, by propagating the corresponding uncertainty sources through the full analysis chain.

As the cross sections are normalised to the inclusive DIS cross section measured in this analysis, some important systematic uncertainties, such as the trigger efficiency, the luminosity and

the uncertainties related to the reconstruction of the scattered positron and of the hadronic final state are largely reduced or cancel. Uncertainties on the measurements of the scattered positron energy (1%) and angle (1 mrad), the energy of the hadronic final state (4%), and the uncertainty on the trigger efficiency (1%) lead to an average combined uncertainty of up to 2%.

The absolute electromagnetic energy scale of the FNC is known to a precision of 5% as described in section 2.2. This leads to an uncertainty of 1% on the cross section measurement at low energies, increasing to 35% for the largest x_L values. The acceptance of the FNC calorimeter is defined by the interaction point and the geometry of the HERA magnets and is determined using MC simulations. The uncertainty of the impact position of the photon on the FNC is due to beam inclination and the uncertainty on the FNC position. It is estimated to be 5 mm. This results in uncertainties on the FNC acceptance determination of up to 15% for the x_L distributions and up to 60% for the p_T^{lead} distribution. These effects are strongly correlated between measurement bins. For the Q^2 and x_{Bj} measurements, these effects lead to normalisation uncertainty of approximately 7%.

The systematic uncertainty arising from the model dependence of the data correction is taken as the difference of the corrections calculated using the LEPTO and CDM models. The resulting uncertainty on the cross-section increases from 1% to 6% for the x_L^{lead} and p_T^{lead} distributions, from 2% to 20% for the x_L^{sum} distribution, and from 1% to 2% for the Q^2 and x_{Bj} distributions. Using different parton distribution functions in the MC simulation results in a negligible change in the cross section.

The systematic errors shown in the figures and table are calculated as the quadratic sum of all contributions, which may vary from point to point. The total systematic error for the normalised cross section measurements ranges between 8% and 18% for x_L^{lead}, 6% and 58% for p_T^{lead}, 8% and 44% for x_L^{sum} and 7% and 8% for Q^2 and x_{Bj}.

3 Results

The measured normalised differential cross sections for the production of very forward photons in the pseudorapidity range $\eta > 7.9$ in DIS in the kinematic range $6 < Q^2 < 100$ GeV^2 and $0.05 < y < 0.6$, are presented in table 1 and figures 3-5. The measurements are presented in figures 3 and 4 as a function of x_L^{lead} and p_T^{lead} of the most energetic photon with $0.1 < x_L^{lead} < 0.7$. The results as a function of the sum of longitudinal momentum fractions x_L^{sum} of all photons with $\eta > 7.9$ are presented in figure 5.

The data are compared with the predictions of models for inclusive DIS (LEPTO and CDM) and models of hadronic interactions (EPOS, SIBYLL and two versions of QGSJET). The ratios of MC model predictions to the measurements are shown separately.

All models tested in this paper overestimate the total rate of forward photons. The LEPTO and CDM models predict about 70% more photons than measured, while EPOS, SIBYLL and QGSJET overestimate the rate of photons by about 30% to 50%. In contrast to the excess of photons in the CDM, the same model predicts a too low rate of forward neutrons as observed in previous H1 analysis of forward neutron production [5].

The shapes of all measured distributions are well described by LEPTO. The CDM predicts harder x_L and p_T spectra. The QGSJET model predicts slightly softer spectra in x_L and p_T. The EPOS and SIBYLL models predict harder x_L spectra, but describe reasonably the shape of p_T distribution.

A measurement of the energy spectra of single photons produced at $\eta > 8.8$ in pp collisions at 7 TeV centre-of-mass energy at the LHC has been recently reported by the LHCf Collaboration [9]. This measurement also shows significant discrepancies with the predictions from hadronic interaction models. However, a direct comparison of the H1 and LHCf results is not possible due to the different kinematic ranges of the two measurements.

The measurement of forward photons allows a test of the limiting fragmentation hypothesis, according to which the production of forward photons in DIS is insensitive to Q^2 and x_{Bj}. To investigate this prediction, the ratio of the forward photon production cross section to the inclusive DIS cross section is measured as a function of Q^2 and x_{Bj} (table 2 and figure 6). Within the uncertainties the fraction of DIS events with forward photons is independent from Q^2 and x_{Bj} in agreement with the limiting fragmentation hypothesis. A similar conclusion was obtained in the earlier H1 analysis of forward neutron production [5]. The LEPTO and CDM predictions also included in figure 6 display a significant difference in normalisation compared to data as well as a slight dependence as a function of Q^2 and x_{Bj}.

4 Summary

The production of high energy forward photons in the pseudorapidity range $\eta > 7.9$ is studied for the first time at HERA in deep-inelastic positron-proton scattering in the kinematic region $6 < Q^2 < 100$ GeV^2, $0.05 < y < 0.6$. The normalised DIS cross sections are presented for the production of the most energetic photon as a function of the longitudinal momentum fraction and transverse momentum in the range $0.1 < x_L^{lead} < 0.7$, and as a function of the sum of longitudinal momentum fractions of all forward photons in the range $0.1 < x_L^{sum} < 0.95$. Predictions of Monte Carlo models overestimate the rate of photons. The shapes of the measured cross sections are well described by the LEPTO MC simulation, while the colour dipole model predicts harder spectra in x_L and p_T. The measurement is also compared to predictions of models which are commonly used for the simulation of cosmic ray air shower cascades. All these models predict different spectra in x_L and p_T. None of the models can describe data in rate and in shape. Within the measured kinematic range, the relative rate of forward photons in DIS events is observed to be independent of Q^2 and x_{Bj}, in agreement with the hypothesis of limiting fragmentation. The present measurement provides new information to further improve the understanding of proton fragmentation in collider and cosmic ray experiments.

Acknowledgements

We are grateful to the HERA machine group whose outstanding efforts have made this experiment possible. We thank the engineers and technicians for their work in constructing and

maintaining the H1 detector, our funding agencies for financial support, the DESY technical staff for continual assistance and the DESY directorate for support and for the hospitality which they extend to the non-DESY members of the collaboration. We also wish to thank Tanguy Pierog and Ralph Engel for providing the predictions of cosmic ray models.

References

[1] C. Adloff *et al.* [H1 Collaboration], Eur. Phys. J. **C6** (1999) 587 [hep-ex/9811013].

[2] S. Chekanov *et al.* [ZEUS Collaboration], Nucl. Phys. **B637** (2002) 3 [hep-ex/0205076].

[3] S. Chekanov *et al.* [ZEUS Collaboration], Nucl. Phys. **B776** (2007) 1 [hep-ex/0702028].

[4] S. Chekanov *et al.* [ZEUS Collaboration], JHEP **06** (2009) 074 [arXiv:0812.2416].

[5] F. D. Aaron *et al.* [H1 Collaboration], Eur. Phys. J. **C68** (2010) 381 [arXiv:1001.0532].

[6] J. Benecke *et al.*, Phys. Rev. **188** (1969) 2159.

[7] T. T. Chou and C.-N. Yang, Phys. Rev. **D50** (1994) 590.

[8] E. Pare *et al.*, Phys. Lett. **B242** (1990) 531.

[9] O. Adriani *et al.* [LHCf Collaboration], CERN-PH-EP-2011-061 [arXiv:1104.5294].

[10] I. Abt *et al.* [H1 Collaboration], Nucl. Instrum. Meth. **A386** (1997) 310.

[11] I. Abt *et al.* [H1 Collaboration], Nucl. Instrum. Meth. **A386** (1997) 348.

[12] R. D. Appuhn *et al.* [H1 SPACAL Group], Nucl. Instrum. Meth. **A386** (1997) 397.

[13] B. Andrieu *et al.* [H1 Calorimeter Group], Nucl. Instrum. Meth. **A336** (1993) 460.

[14] T. Nichols *et al.* [H1 SPACAL Group], Nucl. Instrum. Meth. **A374** (1996) 149.

[15] D. Pitzl *et al.*, Nucl. Instrum. Meth. **A454** (2000) 334 [hep-ex/0002044].

[16] C. Adloff *et al.* [H1 Collaboration], Z. Phys. **C76** (1997) 613 [hep-ex/9708016].

[17] M. Peez, *"Search for deviations from the standard model in high transverse energy processes at the electron proton collider HERA."* (In French), PhD thesis, Univ. Lyon (2003), CPPM-T-2003-04 (available at http://www-h1.desy.de/publications/theses_list.html).

[18] S. Hellwig, *"Investigation of the $D^* - \pi_{slow}$ double tagging method in charm analyses."* (In German), Diploma thesis, Univ. Hamburg (2004) (available at http://www-h1.desy.de/publications/theses_list.html).

[19] R. Brun *et al.*, GEANT3, CERN-DD/EE/84-1.

[20] K. Charchula, G. A. Schuler and H. Spiesberger, DJANGOH 1.4, Comput. Phys. Commun. **81**, 381 (1994).

[21] G. Ingelman, A. Edin and J. Rathsman, LEPTO 6.5, Comput. Phys. Commun. **101** (1997) 108 [hep-ph/9605286].

[22] L. Lönnblad, ARIADNE 4.10, Comput. Phys. Commun. **71** (1992) 15.

[23] B. Andersson *et al.*, Phys. Rept. **97** (1983) 31.

[24] T. Sjostrand, PYTHIA 5.7 and JETSET 7.4, hep-ph/9508391.

[25] A. Kwiatkowski, H. Spiesberger and H. J. Möhring, HERACLES 1.0, Comp. Phys. Commun. **69** (1992) 155.

[26] A. Edin, G. Ingelman and J. Rathsman, Phys. Lett. **B366** (1996) 371 [hep-ph/9508386].

[27] A. Aktas *et al.* [H1 Collaboration], Eur. Phys. J. **C46** (2006) 27 [hep-ex/0508055].

[28] F. D. Aaron *et al.* [H1 Collaboration], Eur. Phys. J. **C64** (2009) 561 [arXiv:0904.3513].

[29] K. Werner, F.-M. Liu and T. Pierog, Phys. Rev. **C74** (2006) 044902 [hep-ph/0506232].

[30] N. N. Kalmykov and S. S. Ostapchenko, Phys. Atom. Nucl. **56** (1993) 346.

[31] N. N. Kalmykov, S. S. Ostapchenko and A. I. Pavlov, Nucl. Phys. Proc. Suppl. **52B** (1997) 17.

[32] S. S. Ostapchenko, Phys. Rev. **D74** (2006) 014026 [hep-ph/0505259].

[33] S. S. Ostapchenko, AIP Conf. Proc. **928** (2007) 118 [arXiv:0706.3784].

[34] J. Engel *et al.*, Phys. Rev. **D46** (1992) 5013.

[35] E.-J. Ahn *et al.*, Phys. Rev. **D80** (2009) 094003 [arXiv:0906.4113].

[36] R. Engel and J. Ranft, PHOJET 1.0, Phys. Rev. **D54** (1996) 4244 [hep-ph/9509373].

x_L^{lead} range	$\frac{1}{\sigma_{DIS}}\frac{d\sigma}{dx_L^{lead}}$	$\delta_{stat.}$	$\delta_{total\ sys.}$	$\delta_{uncorrel.sys.}$	correlated sys. uncertainty		
					$\delta_{E_{FNC}}$	$\delta_{XY_{FNC}}$	δ_{model}
$0.10 \div 0.22$	0.134	0.001	0.011	0.002	0.001	0.011	0.001
$0.22 \div 0.34$	0.0577	0.0005	0.0061	0.0012	0.0029	0.0052	0.0008
$0.34 \div 0.46$	0.0226	0.0003	0.0029	0.0005	0.0018	0.0023	0.0003
$0.46 \div 0.58$	0.00764	0.00017	0.00123	0.00029	0.00061	0.00099	0.00027
$0.58 \div 0.70$	0.00229	0.00008	0.00048	0.00017	0.00025	0.00034	0.00016
p_T^{lead} range [GeV]	$\frac{1}{\sigma_{DIS}}\frac{d\sigma}{dp_T^{lead}}$ [GeV^{-1}]	$\delta_{stat.}$ [GeV^{-1}]	$\delta_{total\ sys.}$ [GeV^{-1}]	$\delta_{uncorrel.sys.}$ [GeV^{-1}]	correlated sys. uncertainty		
					$\delta_{E_{FNC}}$ [GeV^{-1}]	$\delta_{XY_{FNC}}$ [GeV^{-1}]	δ_{model} [GeV^{-1}]
$0.0 \div 0.1$	0.159	0.001	0.010	0.003	0.005	0.008	0.001
$0.1 \div 0.2$	0.0971	0.0010	0.0116	0.0041	0.0068	0.0078	0.0034
$0.2 \div 0.3$	0.0220	0.0005	0.0056	0.0010	0.0024	0.0048	0.0008
$0.3 \div 0.4$	0.00395	0.00029	0.00229	0.00025	0.00087	0.00209	0.00020
x_L^{sum} range	$\frac{1}{\sigma_{DIS}}\frac{d\sigma}{dx_L^{sum}}$	$\delta_{stat.}$	$\delta_{total\ sys.}$	$\delta_{uncorrel.sys.}$	correlated sys. uncertainty		
					$\delta_{E_{FNC}}$	$\delta_{XY_{FNC}}$	δ_{model}
$0.10 \div 0.27$	0.110	0.001	0.009	0.002	0.001	0.009	0.002
$0.27 \div 0.44$	0.0353	0.0003	0.0038	0.0009	0.0018	0.0032	0.0007
$0.44 \div 0.61$	0.0115	0.00021	0.0018	0.0007	0.0009	0.0012	0.0006
$0.61 \div 0.78$	0.00315	0.00011	0.00068	0.00032	0.00032	0.00041	0.00031
$0.78 \div 0.95$	0.000468	0.000039	0.000172	0.000050	0.000140	0.000070	0.000050

Table 1: The normalised cross sections for the production of forward photons in the pseudorapidity range $\eta > 7.9$ in deep-inelastic scattering in the kinematic region $6 < Q^2 < 100$ GeV^2 and $0.05 < y < 0.6$ as a function of the longitudinal momentum fraction x_L^{lead} and transverse momentum p_T^{lead} of the most energetic photon in the energy range $0.1 < x_L^{lead} < 0.7$ and as a function of the sum of the longitudinal momentum fractions of photons x_L^{sum}. For each measurement, the statistical, the total systematic, the uncorrelated systematic uncertainties, and the bin-to-bin correlated systematic uncertainties due to the FNC absolute energy scale, the impact position of the FNC and the model dependence of data correction are given.

Q^2 range $[GeV^2]$	$\frac{\sigma^{\gamma}_{DIS}(Q^2)}{\sigma_{DIS}(Q^2)}$	$\delta_{stat.}$	$\delta_{total\ sys.}$	$\delta_{uncorrel.sys.}$	correlated sys. uncertainty		
					$\delta_{E_{FNC}}$	$\delta_{XY_{FNC}}$	δ_{model}
$6.0 \div 24.8$	0.0276	0.0001	0.0020	0.0003	0.0011	0.0017	0.0001
$24.8 \div 43.6$	0.0265	0.0003	0.0020	0.0003	0.0011	0.0016	0.0001
$43.6 \div 62.4$	0.0265	0.0005	0.0020	0.0004	0.0011	0.0016	0.0001
$62.4 \div 81.2$	0.0261	0.0007	0.0020	0.0005	0.0010	0.0016	0.0001
$81.2 \div 100.0$	0.0279	0.0011	0.0021	0.0005	0.0011	0.0017	0.0001
x_{Bj} range	$\frac{\sigma^{\gamma}_{DIS}(x_{Bj})}{\sigma_{DIS}(x_{Bj})}$	$\delta_{stat.}$	$\delta_{total\ sys.}$	$\delta_{uncorrel.sys.}$	correlated sys. uncertainty		
					δ_{E}	δ_{XY}	δ_{model}
$1.00 \cdot 10^{-4} \div 2.75 \cdot 10^{-4}$	0.0273	0.0003	0.0020	0.0004	0.0011	0.0016	0.0001
$2.75 \cdot 10^{-4} \div 7.69 \cdot 10^{-4}$	0.0275	0.0002	0.0020	0.0003	0.0011	0.0017	0.0001
$7.69 \cdot 10^{-4} \div 2.98 \cdot 10^{-3}$	0.0273	0.0002	0.0020	0.0004	0.0011	0.0016	0.0001
$2.98 \cdot 10^{-3} \div 5.75 \cdot 10^{-3}$	0.0270	0.0003	0.0020	0.0004	0.0011	0.0016	0.0001
$5.75 \cdot 10^{-3} \div 1.58 \cdot 10^{-2}$	0.0276	0.0007	0.0021	0.0006	0.0011	0.0017	0.0001

Table 2: The fraction of DIS events with forward photons in the kinematic region $6 < Q^2 < 100$ GeV^2 and $0.05 < y < 0.6$ and the pseudorapidity of the photon $\eta > 7.9$. For each measurement, the statistical, the total systematic, the uncorrelated systematic uncertainties, and the bin-to-bin correlated systematic uncertainties due to the FNC absolute energy scale, the impact position of the FNC and the model dependence of data correction are given.

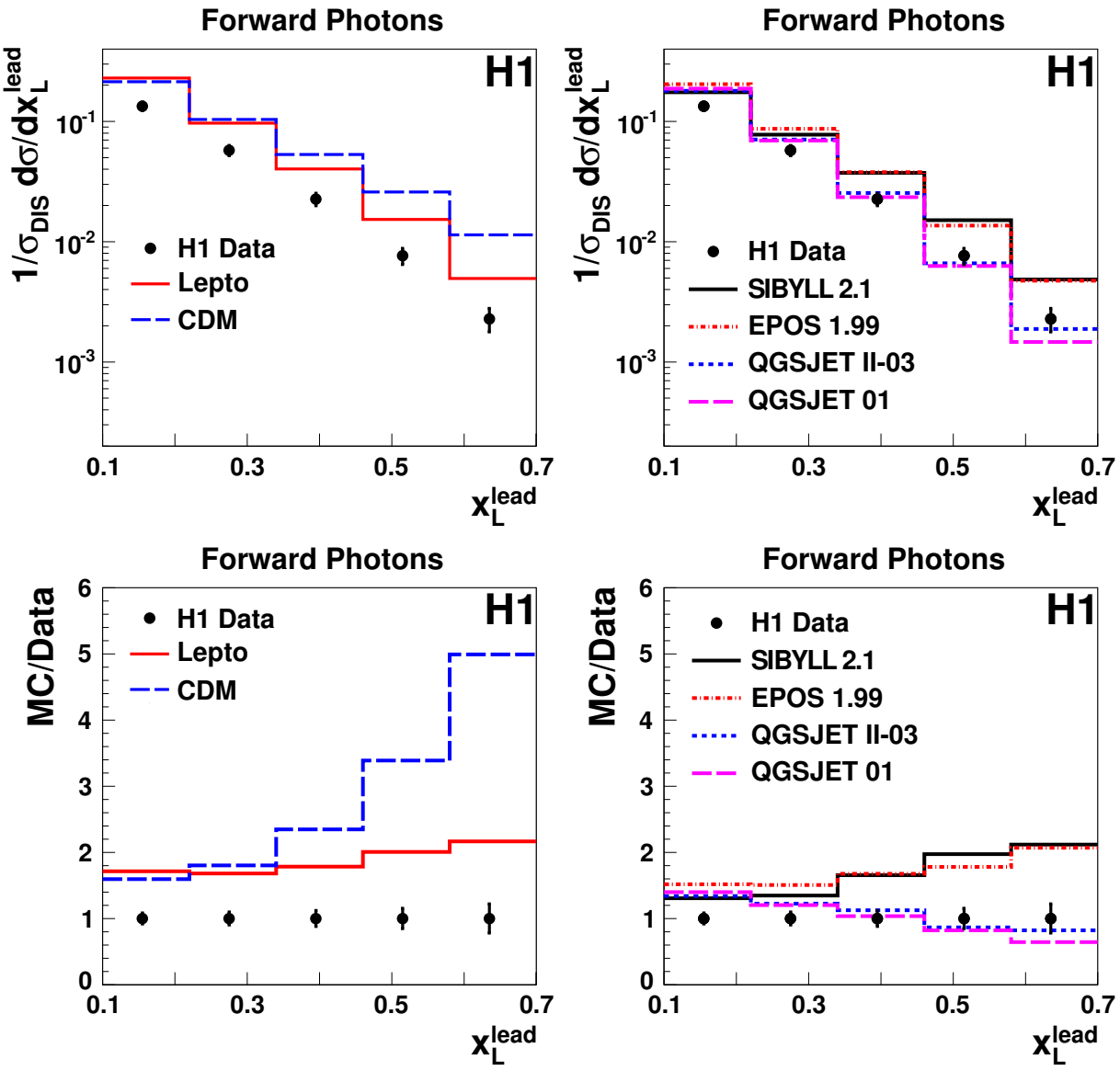

Figure 3: The normalised cross sections for the production of forward photons in the pseudo-rapidity range $\eta > 7.9$ in deep-inelastic scattering in the kinematic region $6 < Q^2 < 100$ GeV^2 and $0.05 < y < 0.6$ as a function of the longitudinal momentum fraction x_L^{lead} of the leading photon in the range $0.1 < x_L^{lead} < 0.7$. The data are compared to two predictions of the DJANGOH Monte Carlo simulation, using LEPTO and CDM to simulate higher orders. Also shown are models of hadronic interactions, QGSJET, EPOS and SIBYLL. The lower row shows the ratios of the Monte Carlo predictions to the data. The error bars show the total experimental uncertainty, defined as the quadratic sum of the statistical and systematic uncertainties.

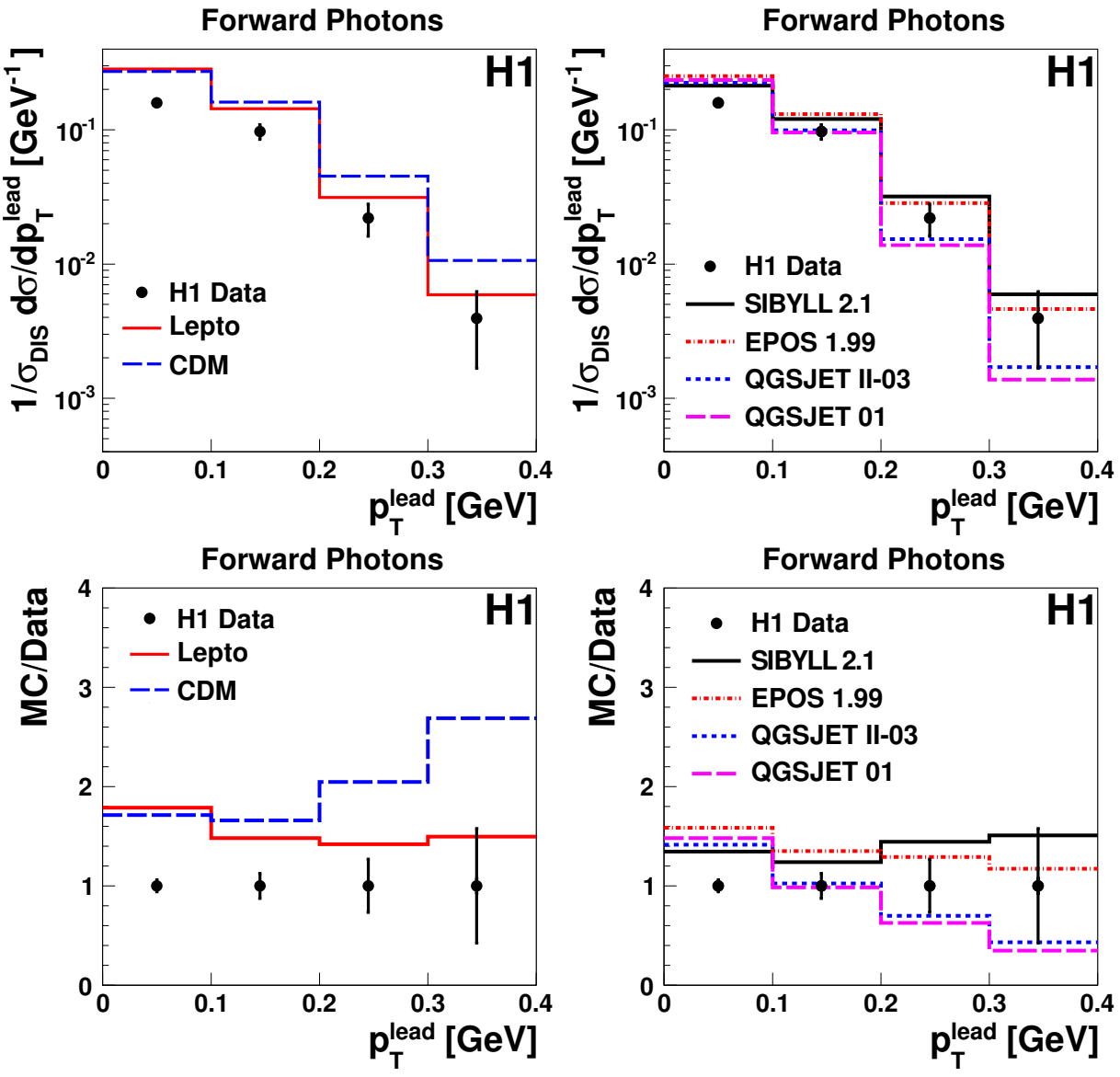

Figure 4: The normalised cross sections for the production of forward photons in the pseudo-rapidity range $\eta > 7.9$ in deep-inelastic scattering in the kinematic region $6 < Q^2 < 100$ GeV^2 and $0.05 < y < 0.6$ as a function of the transverse momentum p_T^{lead} of the leading photon in the energy range $0.1 < x_L^{lead} < 0.7$. The data are compared to two predictions of the DJANGOH Monte Carlo simulation, using LEPTO and CDM to simulate higher orders. Also shown are models of hadronic interactions, QGSJET, EPOS and SIBYLL. The lower row shows the ratios of the Monte Carlo predictions to the data. The error bars show the total experimental uncertainty, defined as the quadratic sum of the statistical and systematic uncertainties.

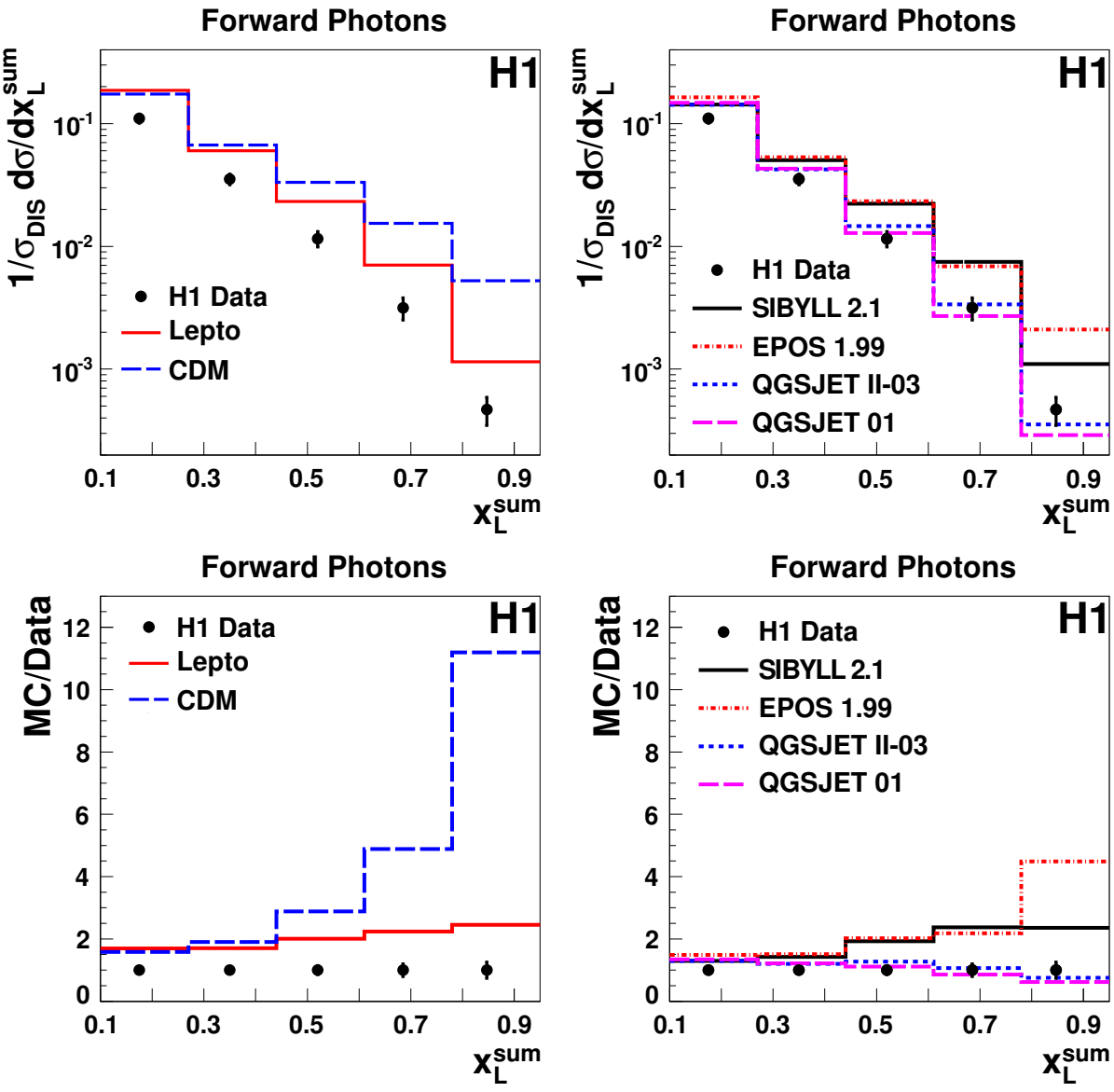

Figure 5: The normalised cross sections for the production of forward photons in the pseudo-rapidity range $\eta > 7.9$ in deep-inelastic scattering in the kinematic region $6 < Q^2 < 100$ GeV^2 and $0.05 < y < 0.6$ as a function of the sum of the longitudinal momentum fractions of photons x_L^{sum}. The data are compared to two predictions of the DJANGOH Monte Carlo simulation, using LEPTO and CDM to simulate higher orders. Also shown are models of hadronic interactions, QGSJET, EPOS and SIBYLL. The lower row shows the ratios of the Monte Carlo predictions to the data. The error bars show the total experimental uncertainty, defined as the quadratic sum of the statistical and systematic uncertainties.

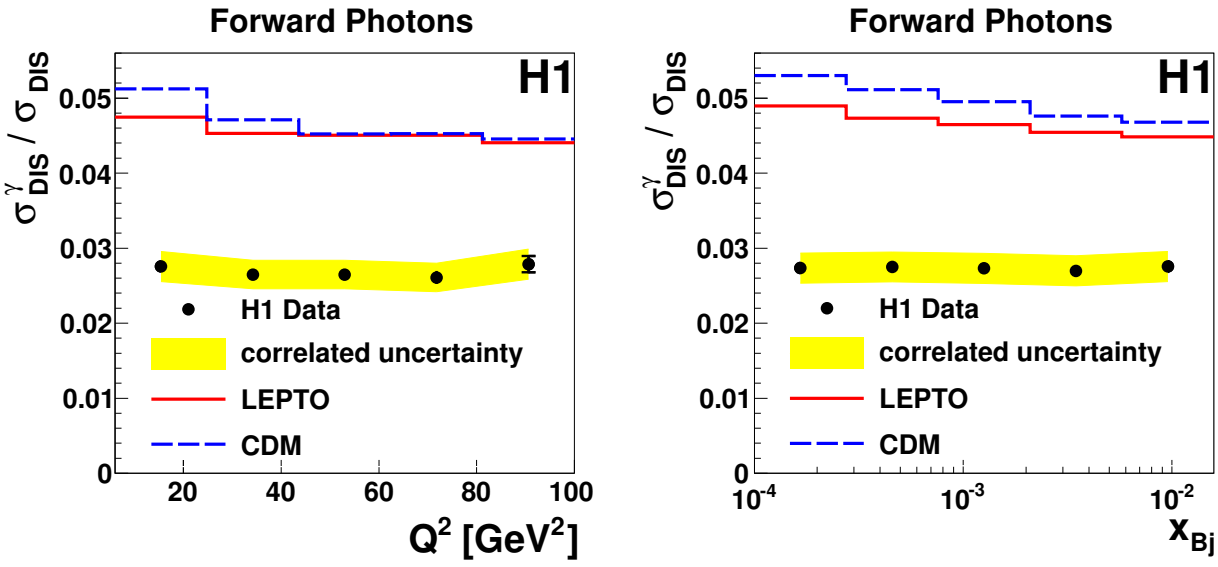

Figure 6: The fraction of DIS events with forward photons in the kinematic region $6 < Q^2 < 100$ GeV^2 and $0.05 < y < 0.6$ and the pseudorapidity of the photon $\eta > 7.9$ as a function of Q^2 and x_{Bj}. The inner error bars shows the quadratic sum of the statistical and the uncorrelated systematic uncertainties. Shaded band shows the correlated systematic uncertainties. The expectation from the LEPTO and CDM models are also shown.